

PAS16

## A Deep Seismic Profile from Noise Records

E.N. Ruigrok\* (Delft University of Technology), X. Campman (Shell International Exploration & Production B.V.) & K. Wapenaar (Delft University of Technology)

### SUMMARY

---

Active-source surveys are widely used for the delineation of hydrocarbon accumulations. Most source and receiver configurations are designed to illuminate the first 5 km of the earth. For a deep understanding of the evolution of the crust, much larger depths need to be illuminated. The use of large-scale active surveys is feasible, but rather costly. As an alternative, we use passive acquisition configurations, aiming at detecting body-wave responses from noise sources, in combination with seismic interferometry (SI). SI refers to the principle of generating new seismic responses by combining seismic observations at different receiver locations.

We studied 40 hours of continuous data, recorded with an array in the Abu Gharadig basin, Egypt. We split up the record in many small time-windows and bandpass filtered the record between 0.4 and 1.0 Hz. It turned out that body waves dominated many noise intervals recorded on the vertical component. By selectively applying seismic interferometry to those noise windows with a favorable illumination, we retrieved P-wave reflection responses. The retrieved shotgathers could straightforwardly be processed into an image. However, we had to add a correction term to account for the angle between the dominant illumination and the array orientation.

## Introduction

The last few years there has been a growing number of body-wave observations in noise records. These body waves are thought to be induced by storms over oceans. When a strong unidirectional wind blows over a water surface, large ocean wavetrains are induced (swell). Under specific conditions this swell can lead to pressure fluctuations at the ocean bottom which leads to the induction of seismic waves. At seismic arrays close to offshore storms especially surface waves are recorded. At arrays far from ocean storms, surface waves would not mask the body-wave signal and hence primarily P-waves would be recorded (Vinnik, 1973). We measured at such an array, in Egypt, and indeed found a large proportion of P-waves.

Also the last few years, a new methodology is under development to image the lithosphere below an array of receivers, without active sources or local earthquakes. Instead, transmitted waves are used which are caused by distant sources. These sources may either be transient or more stationary. With this new methodology, called seismic interferometry (SI), reflection responses are extracted from the coda of transmissions.

Combining the two developments, it is clear that there is a large potential for obtaining reflection responses from low-frequency noise. A potential practical advantage of using noise instead of earthquake responses would be that an array only needs to be deployed for a few days or weeks instead of months, to gather enough illumination.

From the point of view of hydrocarbon exploration, high-resolution seismic reflection data is the most important exploration tool. However, increasingly, companies integrate various types of data to paint a more complete picture of the potential reservoir. In most cases, regional geological information also plays a role in the evaluation of the hydrocarbon potential of a basin. Furthermore, the availability of low-frequency data allows a more successful full-waveform inversion.

It is with these observations in mind that we study a noise record in the frequency range [0.03 40] Hz, recorded with an array in Egypt. We split up the noise in different frequency bands. The division is based on the potentially different origins of the noise for different frequencies. For each frequency band we search for time intervals with primarily body-wave arrivals. In this abstract, we focus on a single frequency band where we found a large proportion of body-wave arrivals. For this frequency band, we will further process the noise records into low-frequency reflectivity images.

## Survey area and geometry

A seismic array was installed in an area over the Northeast Abu Gharadig Basin in the Western Desert in Egypt. This location is about 230 km west of Cairo. While the area is unpopulated, there is some activity related to oil-and-gas production. During the day, several tracks in the area were being used by traffic from local producers. The nighttime was very quiet.

The survey was originally designed to test the application of time-reverse imaging to seismic noise. The goal was to locate local Huygens' sources, as described by Saenger et al. (2009) and Artman et al. (2010). For this reason a quite comprehensive sampling and three-component (3C) seismometers were necessary. We take advantage of this 3C station layout in that we can apply multichannel and multicomponent noise characterization algorithms.

Fig. 1 depicts the receiver layout. 110 broadband seismometers (Trillium T40) were placed in five parallel lines and three cross lines at varying angles. Inline interstation spacing was 500 m, with a more densely sampled (350 m) area in the middle of the array. In total, about 60 hours of noise were simultaneously recorded on all 110 stations. The total survey area was about 60 km<sup>2</sup>.

Most of the stations are installed on a gravel plane. However, between stations 420 and 423 there is one significant sand dune crossing the array. In general, the topography is slightly undulating, but not to the extent that station corrections are required to account for it.

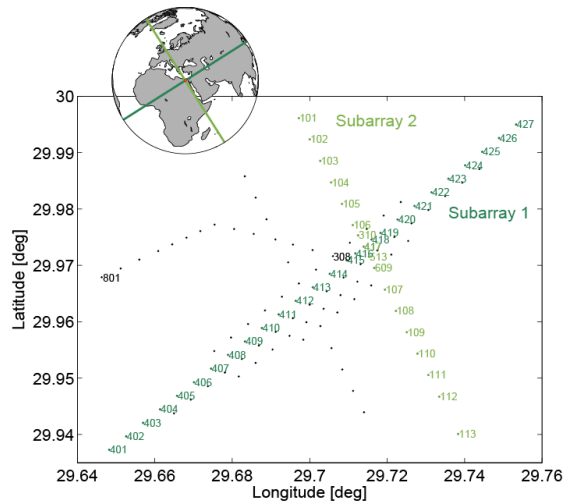


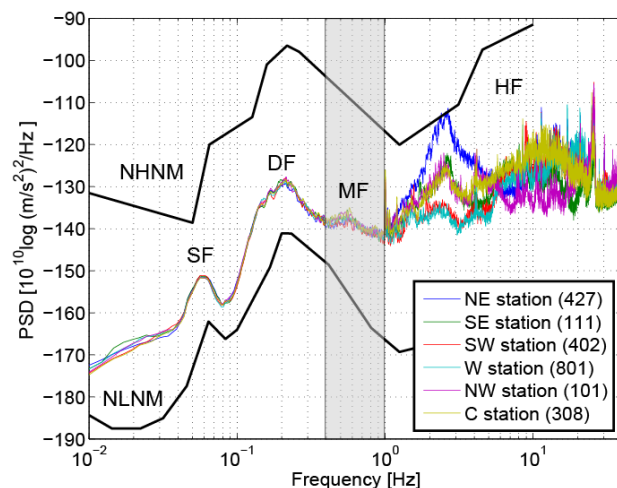
**Figure 1** The Egypt-array configuration. The 110 three-component stations are denoted with black dots. The stations for various subarrays are coloured and numbered. In the inset, the bearings of the different subarrays are shown as rhumb lines on a worldmap.

## Noise analysis for seismic interferometry

From the theory behind SI we know that a favorable source distribution is required to extract meaningful responses from the noise (Wapenaar and Fokkema, 2006). Our primary goal is therefore to characterize the noise and identify - where possible - its source areas, so as to evaluate the illumination of the array.

We restrict our analysis to a 40 hour period, starting October 12 2009, in which all stations were active. For this period, we compare the array measurements with the NLNM (New Low Noise Model) and the NHNM (New High Noise Model) from Peterson (1993). Per station we compute power spectral densities (PSDs) with the recipe given in the above reference. The PSDs for a selected spatial distribution of stations are plotted in Fig. 2.

**Figure 2** Spatial variation of the power spectral densities (PSDs) for the Egypt array. The locations of the stations for which the PSDs were computed can be found in Fig. 1. The PSDs are compared with the new low noise model (NLNM) and new high noise model (NHNM) from Peterson (1993) (solid black lines). The frequency band that is used in this study, the MF band, is marked with gray shading.



We observe a large similarity of the PSDs for the different stations below 1 Hz as opposed to large differences above 1 Hz. Frequencies below the 1 Hz are mostly dominated by natural sources and follow the global trend indicated by the NLNM and NHNM. Two peaks can be identified, the so-called single-frequency (SF) and double-frequency (DF) microseism<sup>1</sup>, at 0.058 and 0.21 Hz,

<sup>1</sup> Note that in seismology the term microseism is used to denote ambient vibrations caused by atmosphere-ocean-solid-Earth interactions. These vibrations are unrelated to microseismics, which are tiny (production-related) earthquakes near hydrocarbon reservoirs.

respectively. Both peaks are related to storms crossing the oceans (Tanimoto & Atru-Lambin, 2007). Such storms are far from the array and hence the similarity of the PSDs for the different stations. Frequencies above 1 Hz, on the other hand, are mostly dominated by anthropogenic sources such as motorized transport and drilling. These sources tend to be much closer to the array and hence the large spatial PSD variations.

Above 1 Hz mostly surface waves are picked up, due to the dominance of anthropogenic, near-surface, sources. Still, the noise may contain a portion of body waves that could, in principle, be isolated for further interferometric processing (Draganov et al., 2009). Our recording, however, lacks the dense station distribution required for suppressing the surface waves from the noise. Hence we restrict our analysis to frequencies below 1 Hz. The frequency band below 1 Hz we split further up in three different bands, the SF, DF and MF band (Fig. 2). For an analysis of all these bands, see Ruigrok et al. (2011). In this abstract we will only focus on the MF band [0.4 – 1.0 Hz], as it is expected that this band will be most relevant one for exploration. In Fig. 2 it can be seen that also in this band the PSDs show a tiny maximum, at about 0.55 Hz, which hints on a noise source different from the SF and DF microseism. For the Egypt array, noise in the MF band comes predominantly from the NNW ( $\sim 315^\circ$ , see Fig. 3c), from the Mediterranean. Hence the naming, ‘Mediterranean Frequencies’.

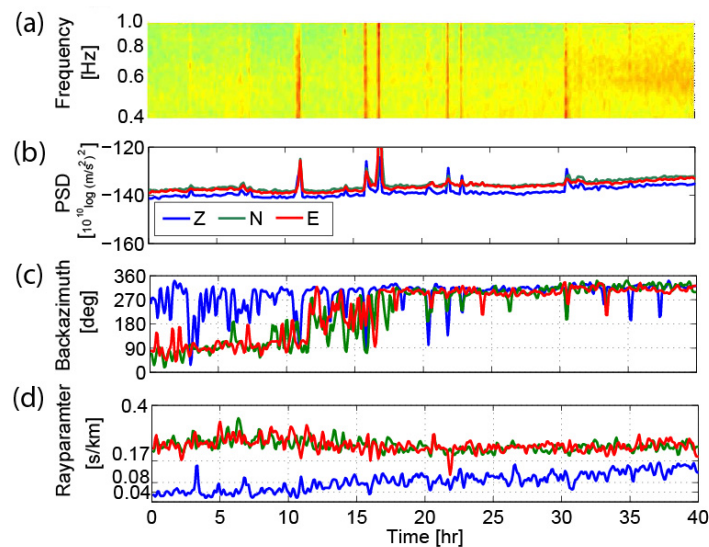


**Figure 3** MF-band noise-variation plots for 40 hours of data, starting 12 October 2009 at 14:00. (a) Power spectrum density (PSD) variation on the vertical component and (b) the summed (over frequency) PSD variation for the vertical (Z)- the North (N)- and the East (E)- components. (c) the dominant backazimuth and (d) the dominant rayparameter variation.

For the noise analysis we split up the 40 hour records in windows of 10 minutes. Using station 402, we compute the PSD for all three components and for all time windows. Fig. 3(a) shows the PSD time-variation plot for the vertical component. Fig. 3(b) is obtained by stacking the PSD time-variation plots over the frequencies within the MF band. The PSD variation functions are shown for the vertical component (Z, blue line), the North component (N, green line) and the East component (E, red line). The peaks in Fig. 3(a) and 3(b) are due to earthquake responses. The other energy is related to noise sources. From about 31 hours an increase in energy can be noted. Overall there is more energy on the horizontal components. This hints on the presence of Love waves.

Fig. 3(c) and 3(d) are the backazimuth and rayparameter time-variation of the dominant waveforms within the noise records. These parameters were estimated by beamforming (Lacoss et al., 1969) 5 minute time windows and selecting the backazimuth  $\theta_{\text{dom}}$  and rayparameter  $p_{\text{dom}}$  with the maximum beampower. During a relatively quiet time, between 0 and 17 hours, the horizontal components pick up noise from different sources than the vertical component, judging the differences in  $\theta_{\text{dom}}(t)$  (Fig. 3c). For the louder times, from 17 hours onwards, all components pick up noise from the same direction.

The  $p_{\text{dom}}(t)$  (Fig. 3d) shows a clear difference between the vertical component (blue line) and the horizontal components (green and red lines). The rayparameters estimated for the Z-component are mostly below 0.12 s/km. These low rayparameters can only be explained with body waves. The

rayparameters increase with time. If we assume a distant source, than the increase in rayparameter can be explained by a source that migrates towards the array. The rayparameters on the horizontal components are significantly larger and can be explained by surface waves between 0 and 17 hours and with a mix of S-phases and surface waves between 17 and 40 hours.

## Processing noise records to images

The exact location of the noise sources is unknown and also not relevant for SI. What is relevant is the effective illumination, which we estimated in Fig. 3(c) and 3(d). The rayparameter distribution estimated for the Z-component is favorable for body-wave SI processing. For this component the illumination is predominantly from the WNW (Fig. 3c). Because subarray 2 has a similar orientation, we first try to reconstruct reflection responses between stations in this subarray.

We parameterize a noise-panel particle-velocity registration  $v$ , as  $v(\mathbf{x}_A, p^+, t)$ , where  $\mathbf{x}_A$  denotes the station location,  $p^+$  is the raytraced dominant rayparameter for a specific time interval and  $t$  is the time variable within the chosen time window. The  $^+$  above the  $p$  denotes that only noise sources from one side of the subarray are considered. For this configuration we can use the following SI relation (Ruigrok et al., 2010):

$$\sum_{p_{\min}^+}^{p_{\max}^+} v(\mathbf{x}_A, p^+, -t) * v(\mathbf{x}_B, p^+, t) \propto G(\mathbf{x}_A, \mathbf{x}_B, t) * S_n(t),$$

where  $G(\mathbf{x}_A, \mathbf{x}_B, t)$  is the impulse response between  $\mathbf{x}_A$  and  $\mathbf{x}_B$ ,  $*$  denotes convolution and  $S_n(t)$  is the average of autocorrelations of the noise.

We further process noise records with  $p_{\text{dom}} < 0.08$  s/km to circumvent pollution with S- and surface waves. For each noise window, all traces are mutually crosscorrelated and crosscorrelations from different noise windows are stacked. The resulting traces are ordered into shotgathers. For each shotgather, the imprint of  $S_n(t)$  is mitigated by applying a source deconvolution. As a deconvolution trace, a time window between -3 and 3 seconds is selected from the virtual source trace, which is the trace that is obtained for  $\mathbf{x}_A$  and  $\mathbf{x}_B$  both at the same station. In total we retrieve as many shotgathers as there are stations (17). Fig. 4 shows five of these shotgathers. The spurious direct waves around  $t=0$  were muted. Until about 7 seconds, a few clear retrieved reflections can be recognized on all panels.

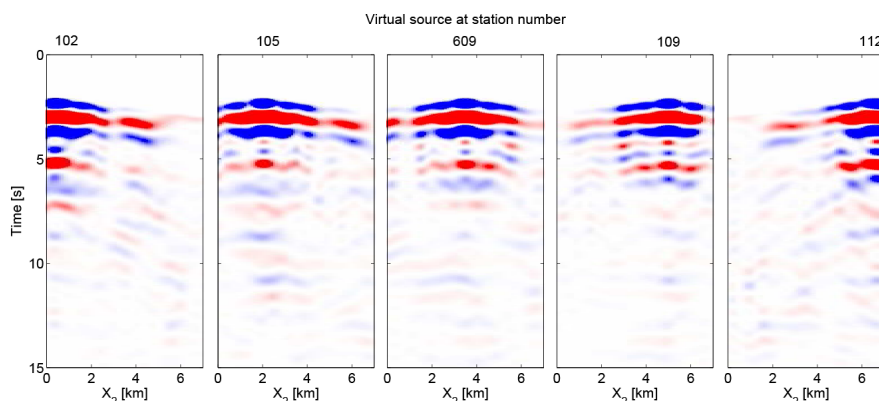


**Figure 4** Retrieved shotgathers for, from left to right, a virtual source at station number 102, 105, 609, 109 and 112, respectively, and receivers on all other station locations of subarray 2 (Fig.1).

The retrieved shotgathers are regularized to station and shot distances of 0.5 km and reordered to common-midpoint (CMP) gathers. Fig. 5(a) shows one such CMP gather. The dotted lines boarder the time-offset range for which reflections with the right kinematics may be expected given illumination with  $p_{\text{max}}=0.08$  s/km (see Ruigrok et al, 2010). Around 3.0 s two-way traveltime (TWT), a clear reflection can be seen. Its blue-red-blue signature is indicative for a positive impedance contrast. This

reflection is overlain by a black hyperbola with  $v_{rms}=3.2$  km/s. At about TWT=6.0 s another reflection can be seen, which might be a multiple of the aforementioned primary reflection, since it has a similar move-out and a reversed polarization.

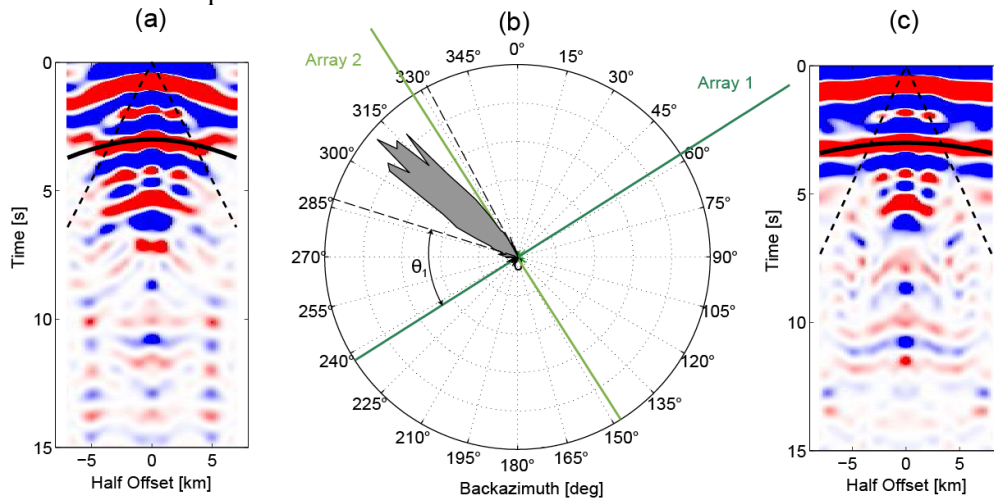


**Figure 5** (a) A common-midpoint (CMP) gather for subarray 2, (b) the orientation of subarray 1 and 2 with respect to the dominant noise illumination (grey shading) and (c) a CMP gather for subarray 1. For both orthogonal CMP gathers the location of the zero-offset trace coincides with the location of station 417 (Fig. 1). On both CMP gathers the first clear reflection is fit with a hyperbola, with (a) 3.2 and (c) 5.0 km/s ( $=3.2/\cos(\theta)$ ), respectively.

Fig. 5(b) depicts the azimuthal distribution of the noise with respect to the orientation of subarrays 1 and 2. Subarray 2 just falls within the illumination range, which borders are highlighted by the broken lines. Subarray 1 has a considerable source-to-subarray azimuth  $\theta$ . Hence, we need to take a different processing approach than for the noise detected with subarray 2. In Ruigrok et al. (2010) SI was applied on earthquake responses detected with a linear array of receivers. Responses from sources that were not in-plane with the receiver array were azimuthally corrected with a  $\cos(\theta)$  term. Here we use the same factor, though in a somewhat different workflow. It is laborious to adjust the move-out of each noise gather with a  $\cos(\theta)$  term based on the beamformed  $\theta_{dom}$ . Instead, we apply the same interferometric processing on the noise records detected with subarray 1 as we did for subarray 2, until we have re-ordered the retrieved shotgathers as CMP gathers. Fig. 5(c) shows a CMP gather for array 1. In Fig. 5(c) the same reflections can be seen as in 5(a). However, the move-outs are different. In Fig. 5(c) apparent root-mean-square velocities  $v_{rms,ap}$  are retrieved instead of actual root-mean-square velocities  $v_{rms}$ . The apparent velocity of the reflection at TWT=3.0 s is well fit by a hyperbola with  $v_{rms,ap}=v_{rms}/\cos(\theta)$ , where  $v_{rms}$  is the velocity estimated for the same reflection in Fig. 5(a) and  $\theta$  is 50 degrees.

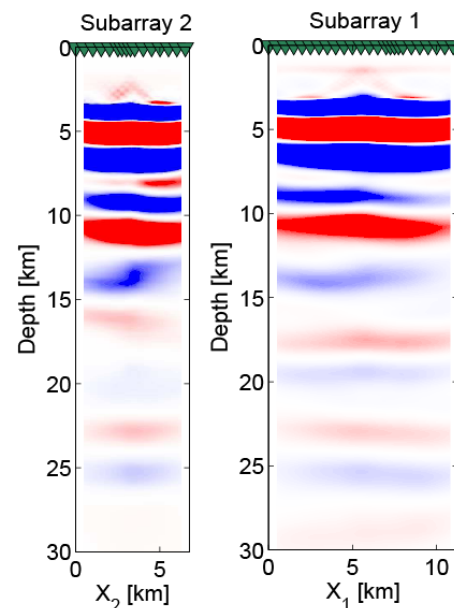


**Figure 6** Post-stack migrated and time-to-depth converted images obtained from MF-band noise records, for subarray 2 (left) and subarray 1 (right).

The CMP gathers are further processed into an image by applying a NMO correction, a poststack time migration and a time-to-depth conversion. The resulting images are shown in Fig. 6(a) and 6(b). For

Fig. 6 (a) and (b) the real and apparent velocities were used for the NMO correction and migration, respectively. Doing so, the reflectors imaged with the two orthogonal subarrays are almost identical, despite the illumination bias for subarray 1. Given the relatively small dimensions of the subarray for the frequencies used, the lateral variations are minimal and in fact 1D profiles are obtained. These profiles can be used to estimate, e.g., the depth of the basin.

## Conclusions

We analysed 40 hours of seismic noise recorded in October 2009 in Egypt. We showed that the Z-component noise, in a frequency band of [0.4 – 1.0] Hz, contains a large proportion of body waves. We used noise time-windows with predominantly steep-angle P-wave arrivals to obtain reflectivity images below two linear subarrays. The obtained images were more or less 1D profiles, due to the limited dimensions of the subarrays for the frequencies used. Until about 20 km depth a few clear reflectors could be identified.

The spatial extent of the array allowed an estimation of the directivity of the incoming noise fields. We showed that the subarray for which we like to obtain an image, does not need to be oriented towards the dominant noise direction. However, the obtained reflection responses need to be move-out corrected using the source-to-subarray azimuth, or further processed with apparent velocities.

## Acknowledgements

This work is supported by The Netherlands Organization for Scientific Research NWO (grant Toptalent 2006 AB) and Shell International Exploration and Production B.V.. We thank Shell Egypt NV for providing the data and for permission to publish the results.

## References

- Artman, B., Podladtchikov, I., and Witten, B. [2010] Source location using time-reverse imaging. *Geophysical Prospecting*, **58**, 861–873.
- Draganov, D., Campman, X., Thorbecke, J., Verdel, A. and Wapenaar, K., [2009] Reflection images from seismic noise. *Geophysics*, **74**, A63–A67.
- Lacoss, R. T., Kelly, E. J., and Toksöz, M. N. [1969] Estimation of seismic noise structure using arrays. *Geophysics*, **34**, 21–38.
- Peterson, J. [1993] Observations and modeling of seismic background noise. USGS Open-File Report 93-322.
- Ruigrok, E., Campman, X., Draganov, D., and Wapenaar, K. [2010] High-resolution lithospheric imaging with seismic interferometry. *Geophysical Journal International*, **183**, 339–357.
- Ruigrok, E., Campman, X. and Wapenaar, K. [2011] Noise analysis for body-wave seismic interferometry. *C.R. Geoscience*, **submitted**.
- Saenger, E., Schmalholz, S., Lambert, M. A., Nguyen, T., Torres, A., Metzger, S., Habiger, R., Miller, T., Rentsch, S., and Mndez-Hernndez, E. [2009] A passive survey over a gas field: analysis of low-frequency anomalies. *Geophysics*, **74**, O29–O40.
- Tanimoto, T. and Atru-Lambin, J. [2007] Interaction of solid-Earth, Atmosphere, and Ionosphere. in: *Earthquake Seismology: Treatise on Geophysics (V. 4)* (H. Kanamari, ed.), Elsevier, 421–444.
- Vinnik, L. [1973] Sources of microseismic P-waves. *Pure and Applied Geophysics*, **103**, 282–289.
- Wapenaar, K. and Fokkema, J. [2006] Green's function representations for seismic interferometry. *Geophysics*, **71**, SI33-SI46.